

Selective Communication for Cooperative Perception in End-to-End Autonomous Driving

Hsu-kuang Chiu¹ and Stephen F. Smith¹

Abstract—The reliability of current autonomous driving systems is often jeopardized in situations when the vehicle’s field-of-view is limited by nearby occluding objects. To mitigate this problem, vehicle-to-vehicle communication to share sensor information among multiple autonomous driving vehicles has been proposed. However, to enable timely processing and use of shared sensor data, it is necessary to constrain communication bandwidth, and prior work has done so by restricting the number of other cooperative vehicles and randomly selecting the subset of vehicles to exchange information with from all those that are within communication range. Although simple and cost effective from a communication perspective, this selection approach suffers from its susceptibility to missing those vehicles that possess the perception information most critical to navigation planning. Inspired by recent multi-agent path finding research, we propose a novel selective communication algorithm for cooperative perception to address this short-coming. Implemented with a lightweight perception network and a previously developed control network, our algorithm is shown to produce higher success rates than a random selection approach on previously studied safety-critical driving scenario simulations, with minimal additional communication overhead.

I. INTRODUCTION

Safety is the most critical concern when deploying autonomous driving systems in the real world. Although autonomous driving technology has advanced dramatically over the past decade due to such factors as the emergence of deep learning and large-scale driving datasets [1]–[5], current state-of-the-art autonomous driving frameworks still have limitations. One principal challenge on the perception side is that the lidar sensors and cameras are usually attached to the roof of an autonomous driving vehicle, and can be occluded by large nearby objects such as trucks or buses. Such perception uncertainty hinders the ability of downstream planning and control processes to make safe driving decisions.

One potential solution to this limited field-of-view problem is cooperative perception: using vehicle-to-vehicle communication to share perception information with other nearby autonomous driving vehicles. Several prior works [6]–[10] have investigated methods for sharing different types of perception information (e.g., lidar point clouds, encoded point features, 3D object detection bounding boxes) to optimize 3D object detection accuracy under communication bandwidth constraints. However, higher 3D object detection accuracy does not always produce better driving decisions and safer driving behaviors. For example, cooperative detection of vehicles that are trailing or moving away from a controlled vehicle will likely not improve overall safety much.

One recent work [8] addresses this evaluation issue by proposing an end-to-end autonomous driving neural network with cooperative perception, applying it to a set of safety-critical driving scenarios within the CARLA [11] autonomous driving system simulator, and measuring the resulting success rates. To respect communication bandwidth constraints, their algorithm limits the scope of cooperative perception with the autonomous vehicle being simulated (referred to hereafter as the *ego-car*) to a subset of the other vehicles within communication range, and this subset is determined through random selection. Because of differences in potential utility of the perception information that can be provided by different nearby vehicles, this approach causes high variance in the output control signals generated and the overall driving success rates obtained. Moreover, this random selection approach may omit those nearby vehicles who possess safety-critical perception information relevant to the ego-car’s planned trajectory and are thus the most informative, as shown in Fig. 1.

Inspired by the idea of *selective communication* in multi-agent path finding research [12], we propose a novel selective communication algorithm for determining the subset of other vehicles that can best cooperatively improve the perception

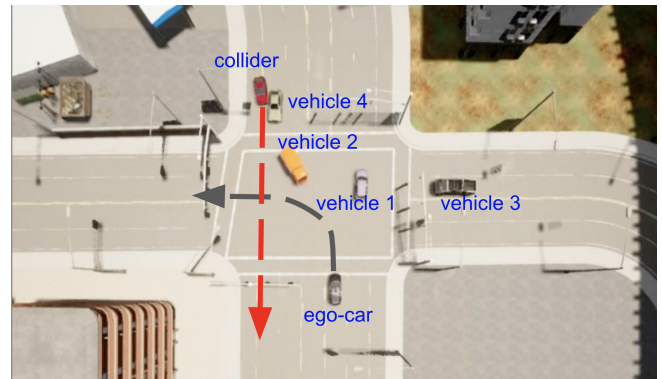


Fig. 1: A potential pre-crash driving scenario. The red car crossing the intersection downward is the potential collider and is not communicating with other vehicles. The grey car is the ego-car being controlled by a driving algorithm and plans to turn left. The yellow truck blocks the ego-car’s line-of-sight and ability to detect the pre-colliding red car. Vehicles 1 ~ 4 can all communicate with the ego-car, but only vehicle 4 can detect the pre-colliding red car given their relative locations. If the ego-car can only select 3 other vehicles to communicate with due to communication bandwidth constraints, the random selection approach has a 25% chance of causing a collision.

¹Carnegie Mellon University, Robotics Institute.

coverage of the ego-car, given the same constraints on subset size. This algorithm is coupled with a lightweight 3D object detector to minimize additional computational cost and communication overhead. We then apply the same driving neural network and evaluation settings as used previously in [8] to show that our selective communication algorithm effectively improves success rates for the set of safety-critical driving scenarios previously considered, with only a small increase in communication bandwidth.

II. RELATED WORK

A. Autonomous Driving

State-of-the-art autonomous driving vehicles [4], [5] operate mainly by executing a sequence of modular functional components, including detection [13]–[15], tracking [16]–[20], prediction [21]–[23], planning [24], and control. This approach provides human-understandable decision-making procedures, but errors may propagate through the systems.

An alternative approach that has emerged more recently in the research community is end-to-end autonomous driving [25], which directly produces the final control signals based on sensor input without performing the aforementioned intermediate tasks. Both the algorithm proposed in [8] and the more informed variant proposed in this paper are instances of this end-to-end approach.

B. Multi-agent Path Finding

The concept of cooperative perception by multiple autonomous vehicles has much in common with variants of multiagent path finding (MAPF) problem [12], [26], and given this similarity, techniques developed to solve these types of MAPF problems can inspire new solutions to cooperative autonomous driving problems. In particular, [12] proposes a decentralized *selective communication* algorithm for a MAPF problem where each agent only has local partial visibility of the navigation environment. Each agent selects other relevant agents in its field-of-view and uses their local observations to produce better path planning.

To be sure, the navigation environment considered in [12] is different than the autonomous driving setting of interest in this paper. It is discretized in both space and time, and each agent’s field-of-view is simply a 2D square region without considering visual occlusion. Nonetheless, the idea underlying this work has inspired our proposed selective communication algorithm for cooperative perception.

C. Cooperative Perception

Given an algorithm for determining the set of other vehicles to communicate with, another important design consideration is what kind of information or data should be communicated from participating vehicles. In [27] the sharing of lidar point clouds with nearby vehicles is advocated. Other research [7], [28] has proposed the sharing of 3D object detection or tracking results. More recent work [8], [9], [29] has favored sharing more efficient, encoded point features, which achieves a good balance between the performance and communication cost and is adopted in this paper. In our proposed selective communication algorithm,

each vehicle first shares relatively sparse center positions of detected objects with the ego-car to determine the subset of vehicles that possess the most useful perception information. Then, in a second round of communication, those selected vehicles share their relatively dense point features with the ego-car for producing its final control signals.

III. METHOD

In the subsections below, we first formally define the problem of interest in this paper. Next we describe our selective communication algorithm. Finally, we summarize the model architectures of the perception neural networks used to assess relative information gain and the control neural networks (drawn from [8]) used to derive control signals.

A. Problem Definition

Given a driving scenario with a static urban environment and a set of other dynamic vehicles (e.g., Fig. 1), we aim to develop a driving algorithm capable of generating control signals that eventually move the ego-car from its starting location to the goal location without colliding with either the environment or other vehicles within a finite time interval. At each time step, the input to the driving algorithm is limited to the ego-car’s encoded lidar observation feature vector O^{ego} and the encoded lidar observation feature vectors ($O^{c_1}, O^{c_2}, \dots, O^{c_{N_c}}$) of N_c selected vehicles.

We define the **selection scope** as :

$$S_s = \{s_1, s_2, \dots, s_{N_s}\}, \quad (1)$$

where each s_i represents the index of a vehicle in ego-car’s communication range. We define the **communication scope** as:

$$S_c = \{c_1, c_2, \dots, c_{N_c}\}, \quad (2)$$

where each c_i represents an index of a vehicle selected to share their encoded observation information with the ego-car. The size of S_s , $|S_s| = N_s$, and the size of S_c , $|S_c| = N_c$, are given as constant parameters.

Our immediate goal is to develop a **selection algorithm** for determining the best subset $S_c \subset S_s$ of vehicles to communicate with. Once determined, the encoded lidar observation features ($O^{c_1}, O^{c_2}, \dots, O^{c_{N_c}}$) of all vehicles in S_c are sent to the ego-car. We also aim to incorporate a **driving algorithm** that takes ($O^{ego}, O^{c_1}, O^{c_2}, \dots, O^{c_{N_c}}$) as input and generates the driving control signals: *throttle* $\in [0, 1]$, *brake* $\in [0, 1]$, and *steer* $\in [-1, 1]$ at each time step.

B. Selective Communication

Our proposed **selective communication algorithm** utilizes two rounds of communication, as shown in Fig. 2. In the first round, each vehicle $s_i \in S_s$ uses its own lidar point cloud input $P^{s_i} \in \mathbb{R}^{N_p \times 3}$ and a lightweight lidar-based 3D object detector to predict the set of objects in its field-of-view, and sends the center locations of all detected objects to the ego-car. Let $D^{s_i} \in \mathbb{R}^{N_d^{s_i} \times N_v}$ represent vehicle s_i ’s internal predicted object detection results, where N_p is the number of lidar points, $N_d^{s_i}$ is the number of detected

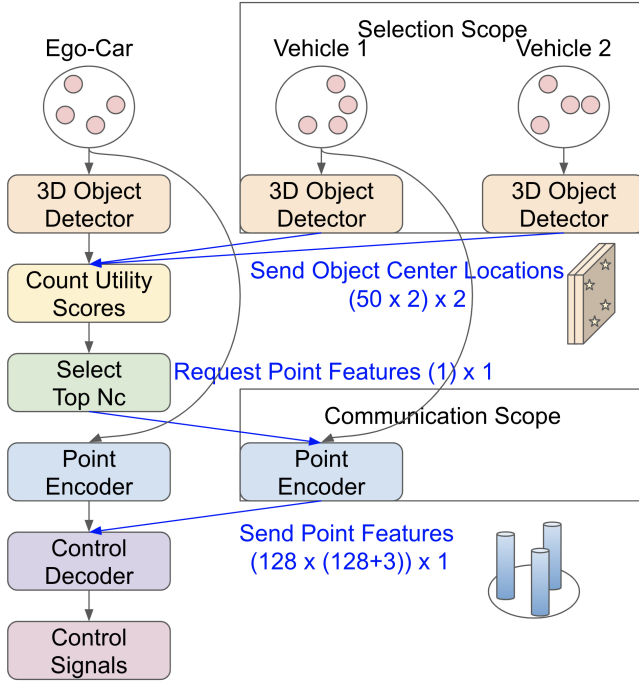


Fig. 2: Two-phase selective communication procedure and control signal generator applied to a minimal example (The numbers shown at each communication step indicate how many floating point numbers are transmitted).

objects, and N_v is the number of variables used to represent a detected object. In our implementation, $N_v = 7$ and the j th detected object $D^{s_i}_j$ can be represented by a vector $[[D^{s_i}_j]_x, [D^{s_i}_j]_y, [D^{s_i}_j]_z, [D^{s_i}_j]_l, [D^{s_i}_j]_w, [D^{s_i}_j]_h, [D^{s_i}_j]_a]$, where $[[D^{s_i}_j]_x, [D^{s_i}_j]_y, [D^{s_i}_j]_z]$ represents the center position, $[[D^{s_i}_j]_l, [D^{s_i}_j]_w, [D^{s_i}_j]_h]$ represents the bounding box size, and $[D^{s_i}_j]_a$ represents the orientation. The $[D]_c$ notation here represents the projection operator that accesses the c column of the matrix D . To minimize communication overhead in the first round, only a subset of this information, specifically only the center locations of detected objects projected to the 2D ground x-y plane, $[D^{s_i}]_{x,y} \in \mathbb{R}^{N_d^{s_i} \times 2}$, are transmitted to the ego-car.

Once this information is received from all vehicles in S_s , the ego-car proceeds to estimate the information gain that would be provided by each prospective communicating vehicle. To do this, the ego-car compares its own set of detected object 2D center positions $[D^{ego}]_{x,y}$ based on its own lidar input $P^{ego} \in \mathbb{R}^{N_p \times 3}$ to the set of detected object 2D center positions $[D^{s_i}]_{x,y}$ received from each vehicle s_i in S_s . We define the **utility score** U^{s_i} of vehicle s_i as the number of objects that s_i detects that are not detected by the ego-car. To simplify the calculation, we assume that s_i 's j th detected object $D^{s_i}_j$ is missed by the ego-car if and only if the 2D center positions of each detected object in $[D^{ego}]_{x,y}$ is at least 0.5 meters away from $[D^{s_i}_j]_{x,y}$. Given this assumption, we define the **utility score** of s_i 's j th detected object as:

$$U^{s_i}_j = I\{d([D^{s_i}_j]_{x,y}, [D^{ego}_k]_{x,y}) > 0.5 \forall k\}, \quad (3)$$

where I is an indicator function, d is the Euclidean distance function, and k is an index of the ego-car's detected object. The overall **utility score** U^{s_i} of vehicle s_i is then just the sum of the utility scores of all its detected objects:

$$U^{s_i} = \sum_{j=1}^{N_d^{s_i}} U^{s_i}_j \quad (4)$$

Once U^{s_i} values have been computed for all $s_i \in S_S$, the vehicles associated with the highest N_c utility scores are selected to form the communication scope S_c .

In the second round of communication, each agent $c_i \in S_c$, upon being requested to, uses a point feature encoder to generate the encoded point feature observation vector O^{c_i} . These point features are then transmitted to the ego-car and used, together with a control neural network, to generate the final control signals.

C. Perception and Control Neural Networks

In this section, we first describe the model architecture of the perception network that is used as the 3D object detector in the first round of communication. Then we will summarize the model of the control network, including both the point feature encoder used by each vehicle in the second round of communication and the control network used in the ego-car to generate the final control signals.

1) *Perception Neural Network*: Instead of using state-of-the-art lidar-based 3D object detectors, we implement a lightweight detector in order not to introduce much computation overhead. The perception neural network we implemented is based on the ideas from Super Fast and Accurate 3D Object Detection (SFA3D) [14] and Real-time Monocular 3D Detection (RTM3D) [15].

Fig. 3 shows the computational pipeline of the implemented perception neural networks. The input point cloud is first voxelized to get a Birds Eye View (BEV) feature map. Then the ResNet18 with Feature Pyramid Network is used to extract an intermediate feature map. Finally, two regression heads containing Conv and ReLU layers are used to produce the center heatmap and the center offset map.

In more detail, each vehicle s_i 's raw lidar point cloud is down-sampled to $N_p = 2048$ points as $P^{s_i} \in \mathbb{R}^{N_p \times 3}$. The input BEV feature map $M_{in}^{s_i} \in \mathbb{R}^{X \times Y \times Z}$ is then generated by voxelizing the 3D space of the driving scene, whose size is $X_m = 140, Y_m = 140, Z_m = 5$ in meters and centered by the agent s_i . The resolution of the voxelization is $dX = dY = dZ = 0.5$ meters, and that infers the shape of the BEV feature map $M_{in}^{s_i}$ is $X = \frac{X_m}{dX} = 280, Y = \frac{Y_m}{dY} = 280, Z = \frac{Z_m}{dZ} = 10$. Each voxel in the BEV map contains a binary value, indicating whether there exist at least 3 lidar points in the voxel. This step can be described by

$$M_{in}^{s_i} = V(P^{s_i}), \quad (5)$$

where V is the voxelization function.

Next, the BEV feature map $M_{in}^{s_i}$ is used as the input to a Keypoint Feature Pyramid Network (KFPN) [15]. It uses ResNet18 [30] with Feature Pyramid Network (FPN)

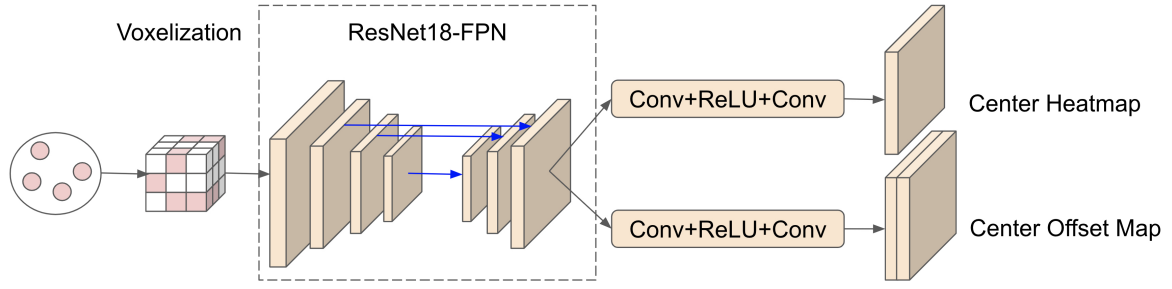


Fig. 3: Perception neural network, used as a lightweight 3D object detector.

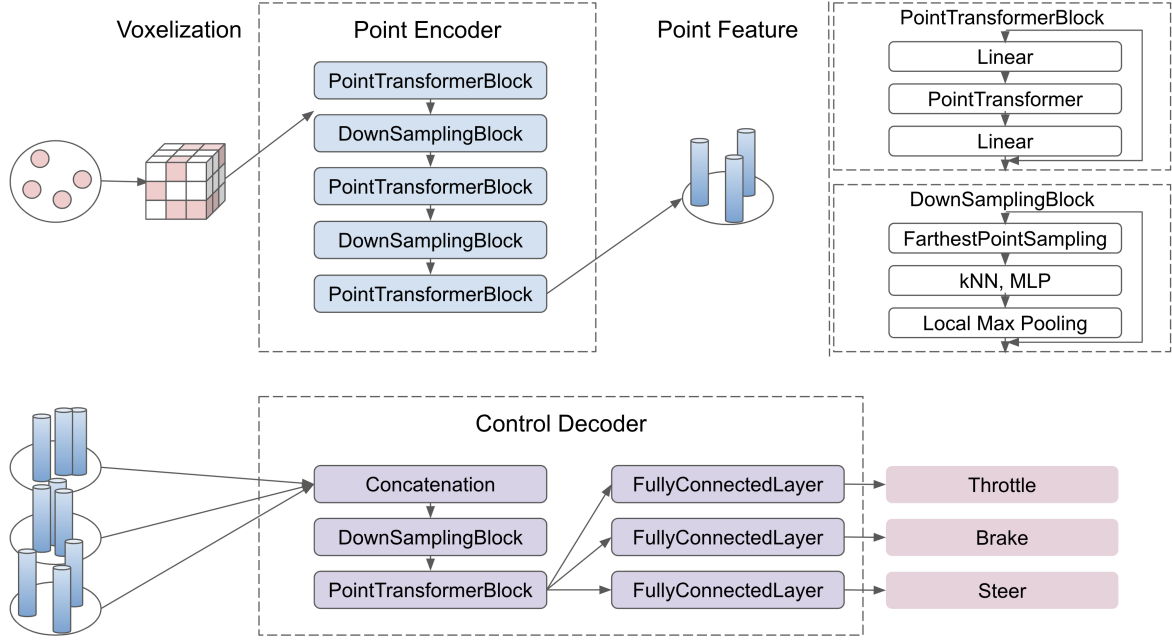


Fig. 4: Control neural network (same as that developed in [8]).

[31] as the feature extraction backbone. This neural network generates an intermediate feature map as follows:

$$M_{inter}^{s_i} = ResNet18FPN(M_{in}^{s_i}), \quad (6)$$

where $M_{inter}^{s_i} \in \mathbb{R}^{\frac{X}{S} \times \frac{Y}{S} \times C}$ represents the intermediate feature map, $S = 4$ is the spatial scale factor, $C = 64$ is the feature channel size. Then the intermediate feature map $M_{inter}^{s_i}$ is used as the input of multiple regression head networks. Each regression head network contains 2 Conv layers and a ReLU layer in between to generate an output map. Different output maps represent different important variables that can be used to construct the object detection result $D^{s_i} \in \mathbb{R}^{N_d^{s_i} \times N_v}$ as defined earlier. Two important regression heads and their output maps are:

$$M_{ch}^{s_i} = R_{ch}(M_{inter}^{s_i}) \quad (7)$$

$$M_{co}^{s_i} = R_{co}(M_{inter}^{s_i}), \quad (8)$$

where $M_{ch}^{s_i} \in [0, 1]^{\frac{X}{S} \times \frac{Y}{S}}$ represents the predicted object center heatmap, R_{ch} is the corresponding regression head neural network, $M_{co}^{s_i} \in \mathbb{R}^{\frac{X}{S} \times \frac{Y}{S} \times 2}$ represents the predicted center offset map, and R_{co} is its regression head neural network.

Given a cell located at (x_{ch}, y_{ch}) in the center heatmap $M_{ch}^{s_i}$ with the predicted object existence probability $M_{ch}^{s_i}[x_{ch}, y_{ch}] > 0$, the corresponding center offset is

$$(x_{co}, y_{co}) = M_{co}^{s_i}(x_{ch}, y_{ch}). \quad (9)$$

The final predicted object 2D center position in the driving scene can be inferred based on the voxelization parameters as follows:

$$[D]x = x_{ch} \times S \times dX - \frac{X_m}{2} + x_{co} \quad (10)$$

$$[D]y = y_{ch} \times S \times dY - \frac{Y_m}{2} + y_{co}. \quad (11)$$

Finally, we set a detection probability threshold value of 0.2 and limit the number of objects detected by any given vehicle $s_i \in S_s$ to a maximum of 50. The loss function we use to train the perception network is the focal loss [32] for the center heatmap $M_{ch}^{s_i}$ and the L1 regression loss for the center offset $M_{co}^{s_i}$. We omit the descriptions of other outputs, such as object size and orientation for simplicity, since those attributes are not used in the downstream process.

2) *Control Neural Network*: To enable a direct comparative basis for quantifying the performance gain due to use of our proposed selective communication model and our simplified lightweight perception network, we adopt the same control neural network that was originally developed in [8], and consider the results presented in this paper as the baseline. Fig. 4 shows the overall architectural diagram. Each vehicle voxelizes the input point cloud and then uses the point transformer [33] block and the downsampling block to get the point feature. The point features derived by each vehicle $c_i \in S_c$ are sent to the ego-car, after which the ego-car uses the control decoder to aggregate those point features and produce the final control signals. For details relevant to reproducing the results presented in the next section, please refer to the Appendix section. For full details of this control neural network, please refer to [8].

IV. EXPERIMENTAL RESULTS

A. Settings

To evaluate our approach to cooperative perception, we follow the same experimental design and evaluation settings utilized in [8]. Three categories of pre-crash driving scenarios from the US National Highway Traffic Safety Administration [34] are configured to construct safety-critical situations caused by visual occlusion as follows:

1) *Overtaking*: As shown in Fig. 5a, a yellow truck remains static in front of the grey ego-car and prevents it from moving forward. The ego-car attempts to overtake by lane changing. However, another red car in the adjacent lane moving in the opposite direction is unable to be detected by the ego-car because the truck blocks the ego-car’s line-of-sight. The arrows show that their planned trajectories will collide if cooperative perception is not applied.

2) *Left turn*: As shown in Fig. 5b, the grey ego-car attempts to turn left in an intersection without a protected left-turn traffic light signal. However, a yellow truck remains static in the intersection waiting for its own left turn. The truck prevents the ego-car from fully perceiving another incoming red car moving in the opposite direction and makes it difficult for the ego-car to determine the right timing for proceeding with the left turn action.

3) *Red light violation*: As shown in Fig. 5c, the grey ego-car attempts to cross an intersection. However, another red car in the horizontal lane ignores its red light signal and continues crossing. Moreover, a yellow truck blocks the ego-car’s ability to detect the traffic rule-violating red car.

In addition to the aforementioned three vehicles involved in the pre-crash scenarios, 30 background vehicles are also introduced into the driving scenarios to produce simulations closer to real-world environments. Note that both the yellow truck and the background traffic participants can share their perception information with the ego-car, while the potential colliding red car can not.

B. Datasets

We use the same training data from [8]’s official website to train our lidar-based 3D object detection model. The

training data contains 12 driving sequences for each of the three scenarios. The data is generated by simulation using an oracle driving policy. This policy uses the ground-truth positions, orientations, sizes, and velocities of all vehicles to predict their future trajectories. Then the A* search algorithm is used to decide how the ego-car should act in every timestep in order to reach its goal without collision.

For evaluation, we again follow the baseline paper [8]. For each of the 3 safety-critical scenarios, 27 driving simulations are performed with 27 different (but fixed) configurations of the attributes of the three main pre-crash relevant vehicles. We repeat each simulation configuration 3 times with different random seeds to vary the starting and ending locations and times of background traffic participants. Both the algorithm of [8] and our proposed variant, which differs only in the use of our two-round selective communication approach to determining S_c instead of [8]’s original random selection approach, are evaluated with selection scope size $|S_s| = 6$ and communication scope size $|S_c| = 3$. Our proposed algorithm variant is also evaluated with $|S_s| = 10$ and $|S_c| = 3$ to examine the performance/communication tradeoff if the selection pool is enlarged.

C. Metrics

Each simulation ends with one of the three outcomes: success, collision, or stagnation. A simulation that is successful means the ego-car reaches its goal location within a limited time. If there is any collision with other agents or the environment, the simulation fails due to collision. If the ego-car is unable to reach the goal within a limited time, the simulation fails due to stagnation. We use success rates as the main evaluation metric. We also show the collision rates and another metric: success rates weighted by completion time (SCT) as follows:

$$SCT = I\{\text{success}\}T_{expert}/T_{model}, \quad (12)$$

where I is an indicator function, T_{expert} is the completion time when simulating with the oracle expert driving policy, and T_{model} is the completion time when using the proposed driving algorithm based on the trained model. Larger SCT indicates that the driving algorithm is more efficient without unnecessary braking.

D. Quantitative Results

1) *Performance*: Table I shows the comparative performance results. We can see that our proposed method (row 2) outperforms the baseline approach of [8] (row 1) by 0.8% ~ 2.1% for the 3 driving scenarios in terms of the success rates. The overall average success rates, success rates weighted by completion time, and collision rates are improved by 1.6%, 0.8%, and 1.1% respectively. We performed a t-test over the binary outcomes produced by both approaches over all simulation runs (i.e., 1 represents success and 0 otherwise), yielding a p-value is 0.066.

Examining the performance difference that results from increasing the size of the selection scope to $|S_s| = 10$ (row 3 of Table I), we see that the overall average success rates,

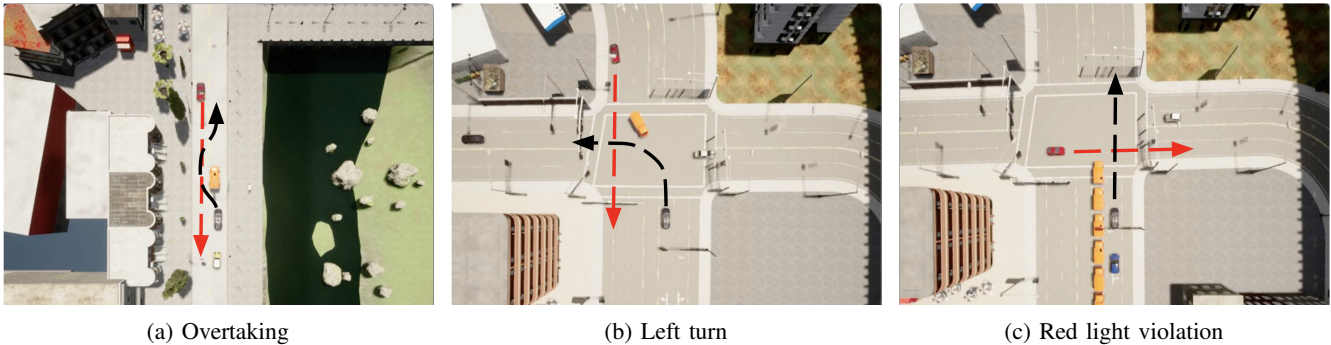


Fig. 5: Examples of the three categories of driving scenarios.

TABLE I: Evaluation results for 3 types of driving scenarios, measuring average Success Rate (SR), Success rate weighted by Completion Time (SCT), Collision Rate (CR), and required bandwidth for single vehicles (single) and all vehicles (total).

Model	Selection Scope Size	Bandwidth (Mbps)		Overtaking			Left Turn			Red Light Violation			Average		
		single	total	SR \uparrow	SCT \uparrow	CR \downarrow	SR \uparrow	SCT \uparrow	CR \downarrow	SR \uparrow	SCT \uparrow	CR \downarrow	SR \uparrow	SCT \uparrow	CR \downarrow
Coopernaut [8]	6	5.10	15.30	90.5	88.4	4.5	80.7	76.2	18.1	80.7	77.8	17.7	84.0	80.8	13.4
Selective Communication (Ours)	6	5.13	15.48	92.6	88.5	6.2	81.5	76.2	16.0	82.7	80.0	14.8	85.6	81.6	12.3
Selective Communication (Ours)	10	5.13	15.60	92.6	89.3	4.9	82.7	77.8	16.0	84.0	81.4	12.3	86.4	82.3	11.1

success rates weighted by completion time, and collision rates improved by 0.8%, 0.7%, and 1.2% respectively.

Overall these results confirm the performance advantage of intelligently selecting vehicles to cooperatively improve perception coverage. They also indicate that this performance advantage can be boosted by expanding the pool of nearby vehicles that are available to select from, suggesting that vehicles closest to the ego-car may also suffer similar perception occlusion problems and not always be the best choice for improving perception coverage. At the same time, these performance gains come at the cost of additional communication and it is important to quantify this tradeoff.

2) *Cost*: The communication bandwidth requirements of each algorithm and configuration evaluated is also reported in Table I. In the baseline case [8], each of the selected 3 vehicles transmits 128 point features. Each point feature is a vector of size $(128+3)$ with 4-byte float numbers. Assuming the frame rate is 10Hz, the communication bandwidth of each vehicle’s transmission is $128 \times (128 + 3) \times 4 \times 10 = 670,720$ bytes per second, or roughly 5.10 mega-bits per second (Mbps), as also reported in the baseline paper [8].

In our selective communication algorithm, each of the 6 vehicles in S_s first transmits (in the worst case) the 2D center positions of all detected objects to the ego-car. Assuming an upper bound of 50 objects, this transmission uses $50 \times 2 \times 4 \times 10 = 4,000$ bytes per second, or roughly 0.03 Mbps. The ego-car then requests the best 3 vehicles to send the point features. Assuming each request can be accomplished by sending a single floating number, this step uses $1 \times 3 \times 4 \times 10 = 120$ bytes per second, which is roughly 0.0009 Mbps. Combining with the bandwidth usage of [8] for transmitting point features in communication round 2, the overall bandwidth requirement of each single vehicle is $0.03 + 0.0009 + 5.10 \approx 5.13$ Mbps, an increase of just 0.6% in communication overhead.

Since more vehicles are involved in communication when using the selective communication algorithm, we also calculate the total amount of data transmitted per second across all

vehicles. In [8], 3 vehicles transmit point features to the ego-car. So the total data transmission is $5.10 \times 3 = 15.30$ Mbps. For the selected communication algorithm, each vehicle in S_s first transmits the 2D center positions of its detected objects to the ego-vehicle, resulting in a total data transmission cost of $0.03 \times 6 = 0.18$ Mbps when $|S_s| = 6$. Requests are then sent from the ego-car to $|S_c| = 3$ vehicles, which costs 0.0009 Mbps as before. Finally, the total cost incurred by these same 3 vehicles sending their point features back to the ego-car is 15.30 Mbps (the same as in [8]). Hence, the the selective communication algorithm’s total data transmission cost for $|S_s| = 6$ is $0.18 + 0.0009 + 15.30 \approx 15.48$ Mbps, an increase of only 1.18% over the baseline approach of [8]. When $|S_s| = 10$, the total data transmission cost increases by 0.78% to $0.03 \times 10 + 0.0009 + 15.30 = 15.60$ Mbps.

E. Qualitative Results

Please refer to the Appendix.

V. CONCLUSION

We propose a novel two-round selective communication algorithm for cooperative perception in end-to-end autonomous driving. In the first round, each vehicle in the ego-car’s communication range performs lightweight 3D object detection and shares the 2D center positions of all detected objects with the ego-car. The ego-car then sorts those vehicles by the provided perception coverage gain and selects the best subset given the communication bandwidth constraints. In the second round of communication, each selected vehicle shares its encoded point transformer features with the ego-car and these features are aggregated to produce the control signals. Our algorithm improves on the success rates achieved by the current state-of-the-art baseline in safety-critical driving scenario simulations, with only slight additional communication cost.

For future work, we are investigating jointly training the perception and control neural networks with a multi-task learning approach.

ACKNOWLEDGEMENT

The research reported in this paper was funded in part by the National Science Foundation under grant #2038612, by the Google cloud research credit program, and by the CMU Robotics Institute.

REFERENCES

- [1] A. Geiger, P. Lenz, and R. Urtasun, "Are we ready for autonomous driving? the kitti vision benchmark suite," in *IEEE/CVF Conference on Computer Vision and Pattern Recognition (CVPR)*, 2012.
- [2] H. Caesar, V. Bankiti, A. H. Lang, S. Vora, V. E. Liong, Q. Xu, A. Krishnan, Y. Pan, G. Baldan, and O. Beijbom, "nuscenes: A multimodal dataset for autonomous driving," *IEEE/CVF Conference on Computer Vision and Pattern Recognition (CVPR)*, 2020.
- [3] M.-F. Chang, J. W. Lambert, P. Sangkloy, J. Singh, S. Bak, A. Hartnett, D. Wang, P. Carr, S. Lucey, D. Ramanan, and J. Hays, "Argoverse: 3d tracking and forecasting with rich maps," in *IEEE/CVF Conference on Computer Vision and Pattern Recognition (CVPR)*, 2019.
- [4] P. Sun, H. Kretschmar, X. Dotiwalla, A. Chouard, V. Patnaik, P. Tsui, J. Guo, Y. Zhou, Y. Chai, B. Caine, V. Vasudevan, W. Han, J. Ngiam, H. Zhao, A. Timofeev, S. Ettinger, M. Krivokon, A. Gao, A. Joshi, Y. Zhang, J. Shlens, Z. Chen, and D. Anguelov, "Scalability in perception for autonomous driving: Waymo open dataset," in *IEEE/CVF Conference on Computer Vision and Pattern Recognition (CVPR)*, June 2020.
- [5] S. Ettinger, S. Cheng, B. Caine, C. Liu, H. Zhao, S. Pradhan, Y. Chai, B. Sapp, C. R. Qi, Y. Zhou, Z. Yang, A. Chouard, P. Sun, J. Ngiam, V. Vasudevan, A. McCauley, J. Shlens, and D. Anguelov, "Large scale interactive motion forecasting for autonomous driving: The waymo open motion dataset," in *IEEE/CVF International Conference on Computer Vision (ICCV)*, October 2021, pp. 9710–9719.
- [6] T.-H. Wang, S. Manivasagam, M. Liang, B. Yang, W. Zeng, J. Tu, and R. Urtasun, "V2vnet: Vehicle-to-vehicle communication for joint perception and prediction," in *European Conference on Computer Vision (ECCV)*, 2020.
- [7] A. Miller, K. Rim, P. Chopra, P. Kelkar, and M. Likhachev, "Cooperative perception and localization for cooperative driving," in *IEEE International Conference on Robotics and Automation (ICRA)*, 2020.
- [8] J. Cui, H. Qiu, D. Chen, P. Stone, and Y. Zhu, "Coopernaut: End-to-end driving with cooperative perception for networked vehicles," in *IEEE/CVF Conference on Computer Vision and Pattern Recognition (CVPR)*, 2022.
- [9] R. Xu, H. Xiang, X. Xia, X. Han, J. Li, and J. Ma, "Opv2v: An open benchmark dataset and fusion pipeline for perception with vehicle-to-vehicle communication," in *IEEE International Conference on Robotics and Automation (ICRA)*, 2022.
- [10] R. Xu, X. Xia, J. Li, H. Li, S. Zhang, Z. Tu, Z. Meng, H. Xiang, X. Dong, R. Song, H. Yu, B. Zhou, and J. Ma, "V2v4real: A real-world large-scale dataset for vehicle-to-vehicle cooperative perception," in *IEEE/CVF Conference on Computer Vision and Pattern Recognition (CVPR)*, 2023.
- [11] A. Dosovitskiy, G. Ros, F. Codevilla, A. Lopez, and V. Koltun, "CARLA: An open urban driving simulator," in *Conference on Robot Learning (CoRL)*, 2017, pp. 1–16.
- [12] Z. Ma, Y. Luo, and J. Pan, "Learning selective communication for multi-agent path finding," *IEEE Robotics and Automation Letters (RAL)*, vol. 7, no. 2, pp. 1455–1462, 2022.
- [13] T. Yin, X. Zhou, and P. Krähenbühl, "Center-based 3d object detection and tracking," in *IEEE/CVF Conference on Computer Vision and Pattern Recognition (CVPR)*, 2021.
- [14] N. M. Dung, "Super-Fast-Accurate-3D-Object-Detection-PyTorch," <https://github.com/maudzong/Super-Fast-Accurate-3D-Object-Detection>, 2020.
- [15] P. Li, H. Zhao, P. Liu, and F. Cao, "Rtm3d: Real-time monocular 3d detection from object keypoints for autonomous driving," in *European Conference on Computer Vision (ECCV)*, 2020.
- [16] R. E. Kalman, "A new approach to linear filtering and prediction problems," *Journal of Basic Engineering*, 1960.
- [17] X. Weng, J. Wang, D. Held, and K. Kitani, "3D Multi-Object Tracking: A Baseline and New Evaluation Metrics," *IEEE/RSJ International Conference on Intelligent Robots and Systems (IROS)*, 2020.
- [18] X. Weng, Y. Wang, Y. Man, and K. Kitani, "Gnn3dmot: Graph neural network for 3d multi-object tracking with multi-feature learning," in *IEEE/CVF Conference on Computer Vision and Pattern Recognition (CVPR)*, 2020.
- [19] H.-k. Chiu, A. Prioletti, J. Li, and J. Bohg, "Probabilistic 3d multi-object tracking for autonomous driving," *arXiv preprint arXiv:2001.05673*, 2020.
- [20] H.-k. Chiu, J. Li, R. Ambrus, and J. Bohg, "Probabilistic 3d multi-modal, multi-object tracking for autonomous driving," *IEEE International Conference on Robotics and Automation (ICRA)*, 2021.
- [21] Y. Chai, B. Sapp, M. Bansal, and D. Anguelov, "Multipath: Multiple probabilistic anchor trajectory hypotheses for behavior prediction," *Conference on Robot Learning (CoRL)*, 2019.
- [22] B. Ivanovic and M. Pavone, "The trajetron: Probabilistic multi-agent trajectory modeling with dynamic spatiotemporal graphs," in *IEEE/CVF International Conference on Computer Vision (ICCV)*, 2019.
- [23] T. Salzmann, B. Ivanovic, P. Chakravarty, and M. Pavone, "Trajetron++: Dynamically-feasible trajectory forecasting with heterogeneous data," in *European Conference on Computer Vision (ECCV)*, 2020.
- [24] E. Bronstein, M. Palatucci, D. Notz, B. White, A. Kuefler, Y. Lu, S. Paul, P. Nikdel, P. Mouglin, H. Chen, J. Fu, A. Abrams, P. Shah, E. Racah, B. Frenkel, S. Whiteson, and D. Anguelov, "Hierarchical model-based imitation learning for planning in autonomous driving," in *IEEE/RSJ International Conference on Intelligent Robots and Systems (IROS)*, 2022.
- [25] M. Bojarski, D. Del Testa, D. Dworakowski, B. Firner, B. Flepp, P. Goyal, L. D. Jackel, M. Monfort, U. Muller, J. Zhang, *et al.*, "End to end learning for self-driving cars," *arXiv preprint arXiv:1604.07316*, 2016.
- [26] J. Li, T. A. Hoang, E. Lin, H. L. Vu, and S. Koenig, "Intersection coordination with priority-based search for autonomous vehicles," in *AAAI Conference on Artificial Intelligence (AAAI)*, 2023.
- [27] E. Arnold, M. Dianati, R. de Temple, and S. Fallah, "Cooperative perception for 3d object detection in driving scenarios using infrastructure sensors," *IEEE Transactions on Intelligent Transportation Systems (T-ITS)*, vol. 23, no. 3, pp. 1852–1864, 2022.
- [28] S. Saxena, I. K. Isukapati, S. F. Smith, and J. M. Dolan, "Multi-agent sensor fusion for connected & autonomous vehicles to enhance navigation safety," in *2019 IEEE Intelligent Transportation Systems Conference (ITSC)*, 2019, pp. 2490–2495.
- [29] Z. Zhang, S. Wang, Y. Hong, L. Zhou, and Q. Hao, "Distributed dynamic map fusion via federated learning for intelligent networked vehicles," in *IEEE International Conference on Robotics and Automation (ICRA)*, 2021, pp. 953–959.
- [30] K. He, X. Zhang, S. Ren, and J. Sun, "Deep residual learning for image recognition," *IEEE/CVF Conference on Computer Vision and Pattern Recognition (CVPR)*, pp. 770–778, 2015.
- [31] T.-Y. Lin, P. Dollár, R. Girshick, K. He, B. Hariharan, and S. Belongie, "Feature pyramid networks for object detection," in *IEEE/CVF Conference on Computer Vision and Pattern Recognition (CVPR)*, 2017, pp. 936–944.
- [32] T.-Y. Lin, P. Goyal, R. Girshick, K. He, and P. Dollár, "Focal loss for dense object detection," in *IEEE/CVF International Conference on Computer Vision (ICCV)*, 2017, pp. 2999–3007.
- [33] L. Zhao, Hengshuang Jiang, J. Jia, P. H. Torr, and V. Koltun, "Point transformer," in *IEEE/CVF International Conference on Computer Vision (ICCV)*, 2021.
- [34] W. G. Najm, R. Ranganathan, G. Srinivasan, J. D. Smith, S. Toma, E. Swanson, and A. Burgett, "Description of light-vehicle pre-crash scenarios for safety applications based on vehicle-to-vehicle communications," in *Technical report, United States. National Highway Traffic Safety Administration*, 2013.
- [35] A. Vaswani, N. Shazeer, N. Parmar, J. Uszkoreit, L. Jones, A. N. Gomez, Ł. Kaiser, and I. Polosukhin, "Attention is all you need," in *Advances in Neural Information Processing Systems (NeurIPS)*, 2017.
- [36] S. Ross, G. Gordon, and D. Bagnell, "A reduction of imitation learning and structured prediction to no-regret online learning," in *International Conference on Artificial Intelligence and Statistics (AISTATS)*, 2011, pp. 627–635.

APPENDIX

A. Control Neural Network (Details)

We adopt the same control neural network architecture from the baseline [8]. As shown in Figure 4, each selected vehicle c_i in the communication scope S_c takes its lidar point cloud $P^{c_i} \in \mathbb{R}^{N_p \times 3}$ as the input of a point cloud encoder neural network E , where $N_p = 2048$ is the number of lidar points. The point cloud encoder E generates the encoded point cloud observation feature O^{c_i} as follows:

$$O^{c_i} = E(P^{c_i}), \quad (13)$$

where $O^{c_i} \in \mathbb{R}^{\frac{N_p}{O_s} \times (O_f + 3)}$, $O_s = 16$ is the point down-sampling factor, $O_f = 128$ is the encoded feature size, and the constant 3 represents that each point's feature vector of a size O_f is appended by the point's 3D position vector. Overall the encoded observation output O^{c_i} can be seen as a set of $\frac{N_p}{O_s}$ key points selected from the original input N_p points, and each selected point contains a feature vector of a size $O_f = 128$ appended with its 3D position.

The point encoder E contains two key components: the down-sampling block and the point transformer [33] block. The down-sampling block contains farthest point sampling, k nearest neighbor finding, multi-layer perceptron, and local max pooling. The main purpose of using the down-sampling block is to select important well-distributed key points from the input point cloud. The point transformer block contains the point transformer and linear layers. This block is used to aggregate important feature vectors from nearby points by an attention neural network [35].

In the second round of communication, each agent c_i in the communication S_c sends its encoded point cloud observation feature $O^{c_i} \in \mathbb{R}^{\frac{N_p}{O_s} \times (O_f + 3)}$ to the ego-car. Then the ego-car concatenates its own encoded point cloud observation feature O^{ego} and all the received features $\{O^{c_i} | c_i \in S_c\}$ as follows:

$$O^{aggr} = \odot(O^{ego}, O^{c_1}, O^{c_2}, \dots, O^{c_{N_c}}) \quad (14)$$

, where $O^{aggr} \in \mathbb{R}^{(\frac{N_p}{O_s}(N_c+1)) \times (O_f + 3)}$ is the aggregated point cloud observation feature, and \odot is the concatenation operator. Then the aggregated feature O^{aggr} is used as the input of the final control decoder F to generate the final control signals as follows:

$$(throttle, brake, steer) = F(O^{aggr}) \quad (15)$$

, where $throttle \in [0, 1]$, $brake \in [0, 1]$, and $steer \in [-1, 1]$ are the vehicle control signals to be applied to the ego-car, F is the final control decoder neural network. The final control decoder also uses the down-sampling block and the point transformer block to model the interaction and correlation among point features from different agents. Finally, three regression heads implemented by fully-connected

neural networks are used to predict the three control signals: *throttle*, *brake*, and *steer* as shown in Figure 4.

The training procedures for the control neural network contains two steps: behavior cloning and data aggregation training [36]. We first run simulations with an oracle expert driving policy to collect the training data for behavior cloning. The oracle expert policy has access to all the obstacle locations and all agents' locations and velocities from the simulator. That information is used to predict other agents' future trajectories and find a collision-free space-time path by the A* search algorithm. The planned space-time path is then transformed to the control signals based on the vehicle dynamics as $(throttle_{oracle}, brake_{oracle}, steer_{oracle})$, which are used as the output part of the training data. The lidar point clouds from the ego-car and the selected vehicles in the communication scope $(P^{ego}, P^{c_1}, P^{c_2}, \dots, P^{c_{N_c}})$ are used as the input part of the training data.

During the training of behavior cloning, we feed the input part of the training data $(P^{ego}, P^{c_1}, P^{c_2}, \dots, P^{c_{N_c}})$ to the control neural network and get the network's output control signals $(throttle_{nn}, brake_{nn}, steer_{nn})$. And we calculate the loss L by the sum of the L1 losses between the control network's output signals and the oracle expert driving policy's control signals as follows:

$$L = |throttle_{nn} - throttle_{oracle}| + \quad (16)$$

$$|brake_{nn} - brake_{oracle}| + \quad (17)$$

$$|steer_{nn} - steer_{oracle}| \quad (18)$$

Once we have the trained model from behavior cloning, we use it as the initialization model for the data aggregation training. In data aggregation training, we iteratively perform interleaving data collection and model training procedures. But the simulation steps in data collection are not always using the oracle expert policy's driving control signals. Instead, there exists an exponentially decayed probability to decide whether to use the control signals from the oracle expert policy or the model being trained. The main motivation of this data aggregation training procedure is to explore more possible scenarios that the current model may experience but the expert policy has not seen before. And the expert policy can provide better control signals for those scenarios as the training data in the next model training iteration.

B. Qualitative Results

The driving video samples of the simulation results using our trained model can be found in the url (<https://youtube.com/playlist?list=PLJdt5JmFddFemsN-8du-TlUXvD6jAznpc>). In general, we can see that the ego-car controlled by our proposed algorithm is aware of other occluded traffic participants and able to make correct driving decisions to avoid collisions.